Generalized far-infrared magneto-optic ellipsometry for semiconductor layer structures: determination of free-carrier effective-mass, mobility, and concentration parameters in *n*-type GaAs

Mathias Schubert and Tino Hofmann

Institut für Experimentelle Physik II, Fakultät für Physik und Geowissenschaften, Universität Leipzig, Linnéstrasse 5, 04103 Leipzig, Germany, and Department of Electrical Engineering, University of Nebraska-Lincoln, Lincoln, Nebraska 68588-0511

Craig M. Herzinger

J. A. Woollam Company, Inc., 645 M Street, Suite 102, Lincoln, Nebraska 68508

We report for the first time on the application of generalized ellipsometry at far-infrared wavelengths (wave numbers from 150 cm^{-1} to 600 cm^{-1}) for measurement of the anisotropic dielectric response of doped polar semiconductors in layered structures within an external magnetic field. Upon determination of normalized Mueller matrix elements and subsequent derivation of the normalized complex Jones reflection matrix **r** of an *n*-type doped GaAs substrate covered by a highly resistive GaAs layer, the spectral dependence of the room-temperature magneto-optic dielectric function tensor of *n*-type GaAs with free-electron concentration of 1.6 $\times$ 10^{18} cm^{-3} at the magnetic field strength of 2.3 T is obtained on a wavelength-by-wavelength basis. These data are in excellent agreement with values predicted by the Drude model. From the magneto-optic generalized ellipsometry measurements of the layered structure, the free-carrier concentration, their optical mobility, the effective-mass parameters, and the sign of the charge carriers can be determined independently, which will be demonstrated. We propose magneto-optic generalized ellipsometry as a novel approach for exploration of free-carrier parameters in complex organic or inorganic semiconducting material heterostructures, regardless of the anisotropic properties of the individual constituents. © 2003 Optical Society of America

OCIS codes: 260.2130, 260.1180, 260.3090.

1. INTRODUCTION

A long-term goal has been the accurate measurement of the "inertial" effective mass[1] m of free carriers with charge q in matter by noncontact optical means. According to the Drude theory, the dielectric function ϵ provides access to the square of the free-charge-carrier (unscreened) plasma frequency ω_p^{*2} and broadening[4] γ_p. Under simplified assumptions about the free-carrier momentum distribution function—single-species carrier plasma taken as an example—ω_p^{*2} and γ_p translate into the coupled quantities N/m and $m\mu$.[2] For determination of the effective mass m and the free-carrier mobility μ, the free-carrier concentration N must be known from a different experiment. Usually, the electrical Hall effect is measured to access N, which requires Ohmic contacts to the sample. No distinction can be made among m, μ, and N from measurement of ϵ alone, nor can the sign of q be differentiated because ω_p^{*2} is proportional to q^2. In a magnetic field, the Lorentz force, an axial vector, diverts the movement of the free-charge carriers, which causes birefringence and which is proportional to both m^{-1} and sgn(q). The dielectric response at optical wavelengths is then a complex tensor $\boldsymbol{\epsilon}$, predicted by the Drude theory (see, e.g., Pidgeon[3]).

In principle, sufficient information is contained within the complex elements of the magneto-optic (MO) $\boldsymbol{\epsilon}$ tensor to differentiate among m, μ, and N and to obtain sgn(q) upon measurement of the tensor element spectra. In essence, to obtain an independent optically determined m, one needs a measurement of the complex-valued birefringence induced by the magnetic field. In semiconductors, the MO birefringence is small at feasible field strength ($\sim$1 T–$\sim$2.5 T) and for typical carrier concentration ($\sim$10^{17} cm^{-3}), effective mass ($\sim$0.1m_0), and mobility values (100–1000 cm^2 V^{-1} s^{-1}), and it vanishes asymptotically for wavelengths $\lambda \rightarrow 0$. However, a small birefringence can measurably affect bulk- and interface-supported eigenmodes (polaritons) in semiconductor layered structures, some of which occur at wavelengths near the coupled longitudinal-optical plasmon–phonon (LPP) mode frequencies, i.e., within the far- or mid-infrared spectral regions.[5–11] The magnetic-field-induced changes of the polariton effects can be measured precisely by polarization-dependent techniques, such as generalized ellipsometry, as will be shown in this work.

Traditional experimental configurations for measurement of MO-induced birefringence effects include normal-incidence-reflection or normal-incidence-transmission

polarized-intensity or polarization rotation spectra with the magnetic field parallel (longitudinal case) or perpendicular (transverse case) to the light propagation. For the transverse case, the incident polarization is either parallel or perpendicular to $\mathbf{B} = \mu_0 \mathbf{H}$. For small m, but with N and μ large, feasible magnetic field strengths can produce clearly measurable effects on the infrared reflectivity, e.g., in n-type InAs at $B = 3.89$ T in transverse MO-plasma reflection.[12] Smaller magnetic fields produce measurable effects on the polarization state of a transmitted wave at frequencies above the LPP modes (Faraday rotation), e.g., in n-type GaAs at $B = 0.833$ T.[13] Such techniques have been used extensively for determination of effective-mass parameters from bulklike semiconductor layered materials, and details shall not be repeated here (see the review by Pidgeon[3] and the references therein). We note, however, that the MO-plasma-reflection technique requires strong fields or small effective-mass values at high concentrations in order to cause measurable changes in the reflected *intensity*. Measurement of Faraday rotation is restricted to samples with a wavelength region of sufficient transparency in order to have light effectively penetrate through the sample, while simultaneously being thick enough for the small MO birefringence to produce measurable rotation of the incident polarization direction and ellipticity (the birefringence becomes smaller at shorter wavelengths).

Neither Kerr reflectivity nor Faraday rotation measurements allow for complete measurement of the complex MO ϵ tensor spectra. In the Voigt configuration, one can, in principle, measure two independent pieces of information: the MO-induced polarization rotation and ellipticity—also known as magnetic double refraction—which provide the cyclotron frequency parameter $\omega_c = q\mu_0 H/m$ according to the Drude model. However, these effects are small and difficult to measure because of the above restrictions.[3] For materials with large m, but small N and μ, or for thin films in layered structures, the MO effects diminish and are difficult to detect experimentally by the above-mentioned techniques. Above all, conductive layers buried by highly resistive materials are completely inaccessible to the electrical Hall-effect measurement.

An alternative is presented here that uses the application of generalized ellipsometry to measure the *complex* MO dielectric tensor elements at far-infrared wavelengths. This requires polarization state measurements and model analysis for oblique angle of incidence. Ellipsometry yields increased precision and additional information (phase) as compared with intensity techniques. This permits measurement of much smaller anisotropy effects, and hence MO effects in materials with lower doping and lower mobility may be detectable, even at room temperature. The generalized ellipsometry approach can handle arbitrarily oriented magnetic field directions, and layered situations in general.[14] Standard (isotropic) ellipsometry determines two independent parameters,[15] which allows for determination of the real and imaginary parts of the isotropic dielectric function ϵ (optical constants $N = n + ik = \sqrt{\epsilon}$), avoiding the Kramers–Kronig extension of pure intensity spectra in order to access the independent parts of the response functions.[16] Generalized ellipsometry determines six parameters related to the optical sample properties,[17] which, upon combination with multiple sample orientation measurements, allows one to differentiate the full set of complex-valued dielectric function tensor elements.[18] Although this has been shown so far for uniaxial absorbing materials only (see, e.g., Refs. 18–20 or recent reviews in Refs. 21 and 22), experiments on biaxial absorbing materials were successful, and reports are under way.[23] This wavelength-by-wavelength ability for exploration of the tensor ϵ offers access to extracting the far-infrared MO tensor ϵ of doped semiconductors regardless of physical assumptions (line-shape models). The spectra obtained on a wavelength-by-wavelength basis can then be compared with the physical line-shape models. This is done here by using the Drude model and, as the substrate, GaAs, for which the free-carrier properties are well-known. Although the Drude model is now established for more than a century, wavelength-by-wavelength-determined complex tensor elements have not been available so far for direct comparison. The agreement obtained here is the most direct proof for the correspondence between the classical Drude model and the optical free-carrier behavior in moderately doped semiconductors at far-infrared wavelengths.

A short introduction of the generalized ellipsometry approach and a brief discussion of the classical free-charge-carrier MO model in semiconductors are given in Section 2. A short description of the model line-shape functions used for the polar lattice response is included. Section 3 outlines the experimental conditions, and results are presented and discussed in Section 4.

2. THEORY

A. Generalized Ellipsometry

Ellipsometry determines the complex ratio ρ of polarized plane-wave components. Traditionally, this ratio is measured in reflection for light polarized parallel (p) and perpendicular (s) to the plane of incidence.[15] The result of an ellipsometry measurement is usually presented through real-valued parameters Ψ and Δ, where $\tan \Psi$ is defined as the absolute value of the complex ratio and Δ denotes the relative phase change of the p and s components of the electric field vector upon interaction with a sample.[15] For nondepolarizing samples, the Jones matrix containing the complex-valued polarized reflection (transmission) coefficients provides a complete description for ellipsometric analysis[15,17,18,24]:

$$\mathbf{r} = \begin{bmatrix} r_{pp} & r_{sp} \\ r_{ps} & r_{ss} \end{bmatrix}. \tag{1}$$

The generalized ellipsometry parameters are then described by three ratios of the four available complex-valued elements of the Jones matrix $\mathbf{r}$.[15,17,18,24–27] Off-diagonal elements are nonzero for optical systems that convert p into s waves, and vice versa. For this work, we have selected the following ratios as the generalized ellipsometry parameters Ψ_{ij}, Δ_{ij} (Ref. 28):

$$\frac{r_{pp}}{r_{ss}} \equiv R_{pp} = \tan \Psi_{pp} \exp(i\Delta_{pp}), \tag{2}$$

$$\frac{r_{ps}}{r_{pp}} \equiv R_{ps} = \tan \Psi_{ps} \exp(i\Delta_{ps}), \tag{3}$$

$$\frac{r_{sp}}{r_{ss}} \equiv R_{sp} = \tan \Psi_{sp} \exp(i\Delta_{sp}). \tag{4}$$

The parameters Ψ and Δ depend on the photon energy $\hbar\omega$, the layer sequence within the sample, each layer's major dielectric function tensor values, each layer's thickness d, the dielectric function of the substrate material that supports the layer stack, the ambient material's dielectric function, and the angle of incidence Φ_a.

An alternative description of the polarized sample response, which can also account for depolarization, is the Mueller matrix and the Stokes vector formalism. In terms of the p- and s-polarized coordinate system of the electromagnetic plane wave, the four real-valued Stokes parameters having dimensions of intensities are expressed as[15] $S_0 = I_p + I_s$, $S_1 = I_p - I_s$, $S_2 = I_{45} - I_{-45}$, and $S_3 = I_{\sigma+} - I_{\sigma-}$, where I_p, I_s, I_{45}, I_{-45}, $I_{\sigma+}$, and $I_{\sigma-}$ denote the intensities for the p-, s-, $+45°$, $-45°$ right-handed circularly, and left-handed circularly polarized light components, respectively.[6,15]

When these elements are arranged into a column vector, the Mueller matrix then describes the changes of each quantity upon interaction of the electromagnetic plane wave with any optical system (sample, mirrors, rotators, etc., and any combinations thereof):

$$\begin{pmatrix} S_0 \\ S_1 \\ S_2 \\ S_3 \end{pmatrix}_{\text{output}} = \begin{bmatrix} M_{11} & M_{12} & M_{13} & M_{14} \\ M_{21} & M_{22} & M_{23} & M_{24} \\ M_{31} & M_{32} & M_{33} & M_{34} \\ M_{41} & M_{42} & M_{43} & M_{44} \end{bmatrix} \begin{pmatrix} S_0 \\ S_1 \\ S_2 \\ S_3 \end{pmatrix}_{\text{input}}. \tag{5}$$

The advantage of this concept is the ability to handle situations with partial depolarization of the electromagnetic plane wave. Details of this concept, its use in ellipsometry, and its relation to the Jones concept have been given previously (see Refs. 6 and 15). For a nondepolarizing system, a one-to-one relation exists between matrices **r** and **M** (Ref. 15):

except for its absolute phase, which can be obtained only by including a compensator(s). Compensators are needed to access the additional Mueller matrix elements.[6]

In principle, because the sample's Jones or Mueller matrix at each wavelength depends on the thickness and the ϵ of each layer, these values can therefore be determined from an ellipsometry experiment by finding the best model that matches calculated data to measured data. Traditionally, wavelength-by-wavelength fits are performed, where the ϵ values of interest are extracted from the experimental data (including data at multiple angles of incidence and at multiple sample azimuths) for each wavelength, independent of all other spectral data points. For this procedure, thickness and ϵ spectra of all other sample constituents have to be known. The dielectric function obtained from the wavelength-by-wavelength fit can then be compared with model assumptions in order to obtain values of physically relevant parameters, such as phonon mode frequencies and broadening parameters. A common, generally more robust procedure is fitting parameterized model dielectric functions (MDFs) to experimental data simultaneously for all spectral data points, which provides a direct connection between measured data and physical parameters of interest. Parametric models further prevent wavelength-by-wavelength measurement noise from becoming part of the extracted dielectric functions and greatly reduce the number of free parameters. In general, one may bypass the intermediate step of obtaining the wavelength-by-wavelength-dependent tensor elements in favor of directly using MDFs to fit for the sample parameters of primary interest.

The standard model for analyzing spectroscopic ellipsometry data is based on a sequence of homogeneous (isotropic or anisotropic) layers with smooth and parallel interfaces. In addition to Ψ, Δ (the standard ellipsometry situation) or Ψ_{pp}, Δ_{pp}, Ψ_{ps}, Δ_{ps}, and Ψ_{sp}, Δ_{sp} (the generalized ellipsometry situation), their standard deviations σ^Ψ, σ^Δ are measured.[29,30] Likewise, when we are working in the Mueller matrix presentation, values for $\sigma^{M_{ij}}$ are obtained by the measurement procedure. When a weighted fitting procedure is used, the standard deviations are propagated appropriately into the error bars on the fit parameters. The light propagation within the sample is calculated by using standard matrix formalism

$$\begin{bmatrix} r_{pp} & r_{sp} \\ r_{ps} & r_{ss} \end{bmatrix}$$

$$\leftrightarrow \begin{bmatrix} \frac{1}{2}(|r_{pp}|^2 + |r_{ss}|^2 + |r_{sp}|^2 + |r_{ps}|^2) & \frac{1}{2}(|r_{pp}|^2 - |r_{ss}|^2 - |r_{sp}|^2 + |r_{ps}|^2) & \mathrm{Re}(r_{pp}\bar{r}_{sp} + \bar{r}_{ss}r_{ps}) & \mathrm{Im}(r_{pp}\bar{r}_{sp} + \bar{r}_{ss}r_{ps}) \\ \frac{1}{2}(|r_{pp}|^2 - |r_{ss}|^2 + |r_{sp}|^2 - |r_{ps}|^2) & \frac{1}{2}(|r_{pp}|^2 + |r_{ss}|^2 - |r_{sp}|^2 - |r_{ps}|^2) & \mathrm{Re}(r_{pp}\bar{r}_{sp} - \bar{r}_{ss}r_{ps}) & \mathrm{Im}(r_{pp}\bar{r}_{sp} - \bar{r}_{ss}r_{ps}) \\ \mathrm{Re}(r_{pp}\bar{r}_{ps} + \bar{r}_{ss}r_{sp}) & \mathrm{Re}(r_{pp}\bar{r}_{ps} - \bar{r}_{ss}r_{sp}) & \mathrm{Re}(r_{pp}\bar{r}_{ss} + r_{ps}r_{sp}) & \mathrm{Im}(r_{pp}\bar{r}_{ss} - r_{ps}r_{sp}) \\ -\mathrm{Im}(r_{pp}\bar{r}_{ps} + \bar{r}_{ss}r_{sp}) & -\mathrm{Im}(r_{pp}\bar{r}_{ps} - \bar{r}_{ss}r_{sp}) & -\mathrm{Im}(r_{pp}\bar{r}_{ss} + \bar{r}_{ps}r_{sp}) & \mathrm{Re}(r_{pp}\bar{r}_{ss} - \bar{r}_{ps}r_{sp}) \end{bmatrix}, \tag{6}$$

where the overbar means the complex conjugate. For the rotating-analyzer system used here, elements in row 4 and column 4 are not measured, which does not impair the accessibility of the normalized Jones matrix elements,

for anisotropic multilayered systems with plane parallel interfaces.[31] Fundamentals of spectroscopic ellipsometry are given by Aspnes[16] and Jellison.[29] Details on generalized ellipsometry are given in Refs. 18, 21, 24, 31, and 32.

Extension of ellipsometry to infrared wavelengths with the Fourier transform infrared technique was pioneered by Röseler[6] and later applied by Henn *et al.*,[33] Kircher *et al.*,[34] Humlíček *et al.*,[35] Tiwald *et al.*,[36] Schubert *et al.*,[37] and Kasic *et al.*[38] for measurement of phonon mode and free-carrier properties of solid-state materials in layered structures. Combination of the Fourier transform infrared ellipsometry approach and the generalized ellipsometry concept was demonstrated recently by Thompson *et al.*,[20] Tiwald and Schubert,[32] and Schubert *et al.*[27]

B. Drude Free-Carrier Magneto-Optic Dielectric Function Tensor

The free-carrier MO contribution to the dielectric tensor $\boldsymbol{\epsilon}$ is obtained through the conductivity tensor $\boldsymbol{\sigma}$ (Refs. 3 and 39):

$$\boldsymbol{\epsilon}^{(\mathrm{FC\text{-}MO})}(\omega) = -\frac{i}{\widetilde{\epsilon}_0 \omega}\boldsymbol{\sigma}, \tag{7}$$

where $\widetilde{\epsilon}_0$ and μ_0 are the vacuum permittivity and permeability and m_0 is the free-electron mass. The components of $\boldsymbol{\sigma}$ in SI units and Cartesian coordinates can be derived from the equation of motion for a free carrier with charge q ($q = +|e|$ for free holes, and $q = -|e|$ for free electrons), anisotropic inverse effective-mass tensor $(m_0\mathbf{m})^{-1}$, and spatially dispersive but energy-independent inverse relaxation time tensor (scattering rate) $\boldsymbol{\gamma}$ when moving in a constant magnetic field $\mathbf{H} = H(h_1, h_2, h_3) = H\mathbf{h}$, with velocity $\mathbf{v} = (\partial_t x, \partial_t y, \partial_t z)$, where $\mathbf{E} = (E_1, E_2, E_3)\exp(i\omega t)$ is the driving field:

$$\mathbf{m}\!\left(\frac{m_0}{q}\right)(\boldsymbol{\gamma} + \partial_t)\mathbf{v} = [\mathbf{E} + \mu_0 H(\mathbf{v}\times\mathbf{h})]. \tag{8}$$

Note that $\mu_{ij} = \mu_{ji}$ and $\gamma_{ij} = \gamma_{ji}$ are assumed here. For isotropic scatter rates, $\gamma_{ii} \equiv \gamma_p$ is the commonly used plasma broadening parameter. Assuming a harmonic plane-wave solution for $\mathbf{v}$ and using Ohm's law $\mathbf{j} = \boldsymbol{\sigma}\mathbf{E} = qN\mathbf{v}$ result in

$$\boldsymbol{\epsilon}^{(\mathrm{FC\text{-}MO})}(\omega) = -\langle\omega_p^{*2}\rangle\Bigg\{(\omega^2\mathbf{I} + i\omega\boldsymbol{\gamma}) - i\omega\langle\omega_c\rangle$$
$$\times\begin{bmatrix} 0 & -h_3 & h_2 \\ h_3 & 0 & -h_1 \\ -h_2 & h_1 & 0 \end{bmatrix}\Bigg\}^{-1}, \tag{9}$$

where the (unscreened) plasma frequency tensor is defined as

$$\langle\omega_p^{*2}\rangle \equiv N\frac{e^2}{\widetilde{\epsilon}_0 m_0}\mathbf{m}^{-1}, \tag{10}$$

which depends on the free-carrier concentration N (free-carrier density) and the free-carrier inverse effective-mass tensor. The free-carrier cyclotron frequency tensor

$$\langle\omega_c\rangle \equiv q\!\left(\frac{\mu_0 H}{m_0}\right)\mathbf{m}^{-1} \tag{11}$$

depends on the magnitude H of the magnetic field, the inverse effective-carrier-mass tensor, and the carrier type. The plasma broadening parameter can be replaced by the optical carrier mobility[2]

$$\gamma_p = \frac{e}{m\mu}. \tag{12}$$

As can be seen from $\boldsymbol{\epsilon}^{(\mathrm{FC\text{-}MO})}$, the magnetic field causes symmetry breaking in $\boldsymbol{\epsilon}$. For $H = 0$, Eq. (9) is identical with the classical Drude equation for one carrier species:

$$\epsilon^{(\mathrm{FC})}(\omega) = -\frac{\langle\omega_p^{*2}\rangle}{\omega(\omega + i\gamma_p)}. \tag{13}$$

It is obvious from Eqs. (10) and (12) that Eq. (13) is sensitive to the coupled quantities N/m and $m\mu$ only (or, equivalently, to N/m and $N\mu$). In Eq. (9), the magnetic field contribution is proportional to the inverse effective-mass tensor elements. With the magnetic field $\mathbf{B} = \mu_0(0, 0, H)$ perpendicular to the sample surface [polar MO (PMO) setup],[40] and for isotropic scattering and inverse effective ("inertial") mass tensors (scalars), the MO Drude tensor simplifies to

$$\boldsymbol{\epsilon}^{(\mathrm{FC\text{-}MO})}(\omega) = \begin{bmatrix} \epsilon_{xx} & i\epsilon_{xy} & 0 \\ -i\epsilon_{xy} & \epsilon_{xx} & 0 \\ 0 & 0 & \epsilon_{zz} \end{bmatrix}, \tag{14}$$

with

$$\epsilon_{xx}(\omega) = -\omega_p^{*2}\frac{\omega + i\gamma_p}{\omega[(\omega + i\gamma_p)^2 - \omega_c^2]}, \tag{15}$$

$$\epsilon_{zz}(\omega) = -\omega_p^{*2}\frac{1}{\omega(\omega + i\gamma_p)}, \tag{16}$$

$$\epsilon_{xy}(\omega) = -\omega_p^{*2}\frac{\omega_c}{\omega[(\omega + i\gamma_p)^2 - \omega_c^2]}. \tag{17}$$

The antisymmetric tensor element ϵ_{xy} depends linearly on $\omega_c = \mu_0 H(q/m)$, which provides sensitivity to q/m. The in-plane component ϵ_{xx} determines ω_p^* and γ_p. The out-of-plane component ϵ_{zz} is identical with $\epsilon^{(\mathrm{FC})}$ without magnetic field and is best measured before the MO experiment. Resonance will occur for $\omega \sim \omega_c$, provided that $\omega_c \gg \gamma_p$. Typical frequencies of ω_c are within the microwave region, where cyclotron resonance absorption can be observed, usually at low temperatures to meet the condition $\omega_c/\gamma_p \gg 1$. For $\omega \gg \omega_c$, however, ϵ_{xy} is asymptotic and approaches 0 for $\omega \to \infty$. A subtle but finite birefringence remains at infrared wavelengths, its strength being dependent on m, μ, and N and its sign dependent on sgn(q) and the orientation of $\mathbf{H}$. This birefringence causes the polarization-dependent MO re-

sponse, which, if detected by the generalized ellipsometry experiment, can be traced back to the model parameters m, μ, N, and sgn(q).

C. Polar Lattice Contributions to the Dielectric Function Tensor

A harmonic oscillator line shape with Lorentzian broadening is employed for calculation of the (isotropic) lattice contribution to ϵ of GaAs (Ref. 42):

$$\epsilon^L = \epsilon_\infty \frac{\omega_{\mathrm{LO}}^2 - \omega^2 - i\omega\gamma}{\omega_{\mathrm{TO}}^2 - \omega^2 - i\omega\gamma}, \qquad (18)$$

where ω_{TO}, ω_{LO}, and γ are the transverse-optical (TO) phonon frequency, longitudinal-optical (LO) phonon frequency, and broadening parameters, respectively. The high-frequency dielectric limit parameter ϵ_∞ accounts for high-energy electronic contributions.[3]

D. Surface Polaritons

The infrared optical response of layered structures composed of polar semiconductor materials is affected by interface mode excitations [surface polaritons (SPs), surface guided waves (SGWs)], where electromagnetic radiation is mediated parallel to the interfaces of thin-film structures.[5] Interface modes are tied to the existence of a surface between two media of certain dielectric properties. SGWs have transverse electric radiation fields (electric field vector parallel to interface). Such effects characterize Brewster modes (total internal reflection) and guided slab modes. SPs possess transverse magnetic fields (magnetic field vector parallel to interface).[43] The denominators of the Fresnel reflection coefficient for p- and s-polarized light provide convenient access to the dispersion for SP and SGW modes in thin-film heterostructures.[5] A detailed treatment of these effects is beyond the scope of the present paper, and the interested reader is referred to existing literature.[5,6,43] The effects of coupled plasmon–phonon–magnon polaritons and splitting of bulk and interface dispersion branches have been studied in theory for surfaces between half-infinite anisotropic (MO) polar semiconductor materials by the group consisting of Wallis, Brion, Burstein, and Hartstein.[7–10] The case studied here by experiment has not been treated yet and shall be the subject of further work. These coupled modes produce well-observable polarization effects *near* the frequencies of the LPP modes, i.e., within the far-infrared spectral region, as will be shown further below.

3. EXPERIMENT

A prototype far-infrared ellipsometer setup at the University of Nebraska-Lincoln was calibrated with the necessary precision required for acquisition of generalized ellipsometry parameters. The ellipsometer was operating in the rotating analyzer ellipsometer configuration with an adjustable polarizer.[15] The focal length of the mirror, which directed the incidence beam onto the sample, was 190 mm, with a typical aperture of 3°. A Nicolet Fourier transform infrared spectrometer was used as the monochromatic light source. As a result of the ellipsometric

measurement, the Mueller matrix elements M_{12}, M_{13}, M_{21}, M_{22}, M_{23}, M_{31}, M_{32}, and M_{33}, normalized to the element M_{11}, were reported.

A Helmholtz-type electromagnet was attached to the ellipsometer. The coils of the magnet were water cooled, and the current through the coils was controlled to maintain constant magnetic fields during the measurements. The strength of the field between the poles was tunable from $\mu_0 H = -2.3\,\mathrm{T}$ to $+2.3\,\mathrm{T}$, with its direction normal to the sample surface. The gap between the pole caps was approximately 4 mm. The strength of the magnetic field between the poles was measured by an electrical Hall probe.

A moderately Te-doped GaAs wafer with nominal free-electron concentration of $N = (1.5 \pm 0.15) \times 10^{18}\,\mathrm{cm}^{-3}$ was taken here as an example. The epi-ready wafer was capped by an undoped GaAs buffer layer with nominal thickness of $d \sim 700\,\mathrm{nm}$ by using metal-organic vapor phase epitaxy and standard growth regimes.

The measurements were performed in a three-step procedure. First, the sample was measured without the magnet at an angle of incidence of $\Phi_a = 80°$. Then the magnet was attached to the ellipsometer. The two arms of the ellipsometer were set to the straight-through (180°) position. Two mirrors were included in the light path in order to redirect the incident beam onto the sample and the exit beam into the detector (see Fig. 1). The mirrors M1 and M2 consisted of smooth gold-coated silicon wafers. Their optical properties were determined before the experiment described here. The mirrors were adjusted to obtain approximately $\Phi_a = 80°$ at the sample, and the measurement was repeated with the magnetic field turned off. The third step was to repeat the measurement, once with the magnetic field set to $\mu_0 H = +2.3\,\mathrm{T}$ and once again with $\mu_0 H = -2.3\,\mathrm{T}$.

4. RESULTS AND DISCUSSION

Before discussion of the MO results, we will first describe how the sample properties were determined from the ellipsometric measurement. Three different approaches were pursued. Approach A consisted in matching experimental and calculated Mueller matrix spectra for the mirror–sample–mirror system by using the MDF for ϵ as described in Section 2. Approach B consisted in wavelength-by-wavelength extraction of the MO dielectric function tensor elements of the GaAs substrate. The results of both approaches (MDF and wavelength-by-wavelength-derived ϵ spectra) were then compared. As
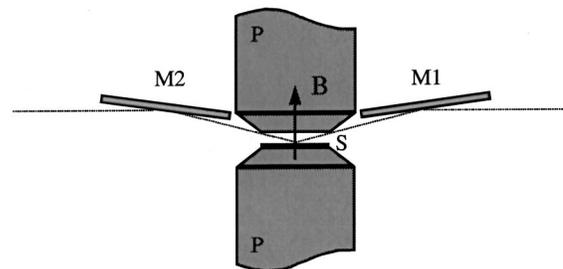

Fig. 1. Schematic drawing (not to scale) of the light path through the magnet (solid line): M1, entrance mirror; M2, exit mirror; S, sample; P, magnet poles; B, magnetic field direction.

an alternative (approach C), instead of matching Mueller matrix element spectra, we also extracted the generalized ellipsometry parameters for the sample alone and compared those with the model calculations from approach A.

Approach A. The Mueller matrix spectra without the magnet were used to find the best-fit parameters for the GaAs MDF parameters and thickness of the epi-layer (ω_{TO}, ω_{LO}, and γ, common to both substrate and buffer layer, in excellent agreement with Ref. 41; ω_p^* and γ_p for the substrate and d for the film, as given in Table 1). The calculated data were obtained by using Eqs. (15)–(17), and Eq. (18) for parameterization of ϵ, and the explicit 4×4 matrix formalism for treatment of light propagation in anisotropic stratified media, where the effect of the i-GaAs buffer layer was considered appropriately.[21] The second measurement (magnet attached, field off) was used to determine the effects of angular rotations and p- and s-amplitude changes imposed by the two Au mirrors. This was done by using the MDF parameters obtained from the first step for calculating the actual sample response and then by fitting the parameters of the corresponding Mueller matrices for mirror effects.[6,15] The experimental and best-fit calculated Mueller matrix element spectra for this step are shown in Fig. 2. Note that all spectra are normalized to the element M_{11} (M_{11} is 1 and not shown). As a result, we obtained the spatial rotations of the light beam's coordinate system on each mirror reflection, the angle of incidence at the sample surface (angle between the infrared light beam axis and the sample normal, $\Phi_a = 80.0° \pm 0.5°$), and at each mirror face. The Mueller matrix element spectra from the third step (magnetic field on) and the differences between spectra at $\mu_0 H = 2.3\,\mathrm{T}$ and $H = 0$ ($\mu_0 \delta H = 2.3\,\mathrm{T}$; Fig. 3) and $\mu_0 H = -2.3\,\mathrm{T}$ and $H = 0$ ($\mu_0 \delta H = -2.3\,\mathrm{T}$; not shown) were then used to differentiate among m, μ, and N. We included the difference spectra in order to more directly isolate the magnetic-field-induced effects. The parameters ω_p^*, ω_c, and γ_p were substituted through Eqs. (10)–(12). The numerical results for N, m, and μ are given in Table 1. The MDF spectra for the GaAs MO ϵ tensor elements are shown in Fig. 4.

Approach B. For the wavelength-by-wavelength procedure, we assumed that the mirror effects, the angle of incidence, the epi-layer thickness, and the epi-layer ϵ obtained by the first procedure were known and sufficiently correct. We justified this assumption because all of these parameters were gained from a field-free measurement. We then fitted the complex-valued elements ϵ_{xx}, ϵ_{zz}, and ϵ_{xy} wavelength by wavelength to all experimental spectra simultaneously (setting $\epsilon_{xx} = \epsilon_{zz}$ and $\epsilon_{xy} = 0$ for spectra with $H = 0$). The wavelength-by-wavelength-fitted ϵ_{xx} and ϵ_{xy} spectra are shown in Fig. 4. The differences be-

tween ϵ_{xx} and ϵ_{zz} at $\mu_0 H = 2.3\,\mathrm{T}$ are too small to be seen at this scale, and the presentation of ϵ_{zz} is therefore omitted for brevity. The most important spectra here are those for the real and imaginary parts of ϵ_{xy}, which decay asymptotically for $\lambda \to 0$, as expected. The wavelength-by-wavelength-obtained spectra are in very good agreement with the MO Drude MDF (solid curves), particularly for ϵ_{xy}.

Approach C. The generalized ellipsometry spectra (the normalized Jones matrix elements) depict the actual sample properties. An alternative approach is therefore to extract these elements from the Mueller matrix by considering the mirror effects as described above. The "experimental" generalized ellipsometry spectra obtained thereby are shown in Figs. 5 and 6 as dotted curves. The spectra were extracted from the Mueller matrix spectra shown in Figs. 2 and 3. Excellent agreement between model line shape (calculated from the model obtained in approach A) and experimental data is achieved. The upper set of curves in Figs. 5 and 6 depicts data without ex-
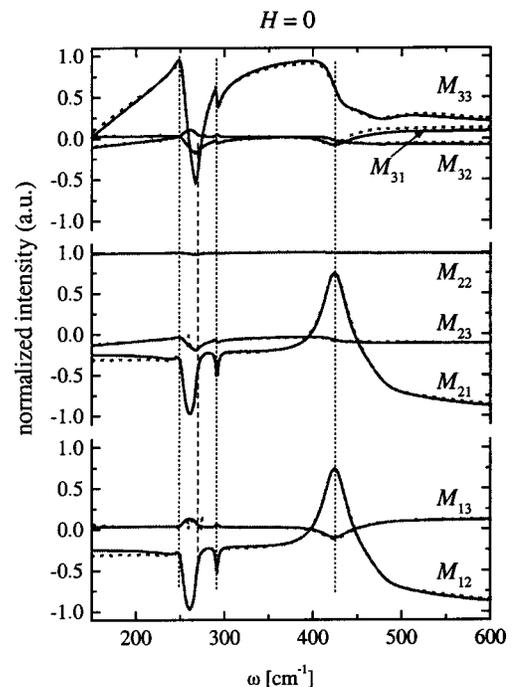

Fig. 2. Experimental (dotted curves) and best-fit (solid curves) far-infrared Mueller matrix spectra obtained by generalized (Mueller matrix) ellipsometry for an i-GaAs(d)/n-GaAs homostructure at $\Phi_a = 80°$, affected by two mirror reflections (before and after the sample, as indicated in Fig. 1). Dotted vertical lines indicate frequencies of the interface modes FSP, SGW$^+$, and SGW$^-$, discussed in the text. The dashed vertical line denotes the wave number of the GaAs TO frequency.

Table 1. Lattice [Eq. (18)], Free-Carrier [Eq. (13)], and MO MDF [Eqs. (15)−(17)] Best-Fit Parameters for the i-GaAs(d)-n-GaAs Layer Structure[a]

ω_{TO} (cm^{-1})	ω_{LO} (cm^{-1})	γ (cm^{-1})	ϵ_∞	ω_p^* (cm^{-1})	γ_p (cm^{-1})	N (10^{18} cm^{-3})	m (m_0)	μ [cm^2/(V s)]
268.0(1)	291.0(1)	3.2(1)	11[b]	1527(3)	57(1)	1.60(5)	0.072(1)	2200(20)

[a] The best-fit thickness was $d = 686(5)$ nm. The value in parentheses represents the 90% confidence interval for the last digit(s).
[b] This value was taken from the compilation given in Ref. 41 and not further varied during the ellipsometry data analysis.
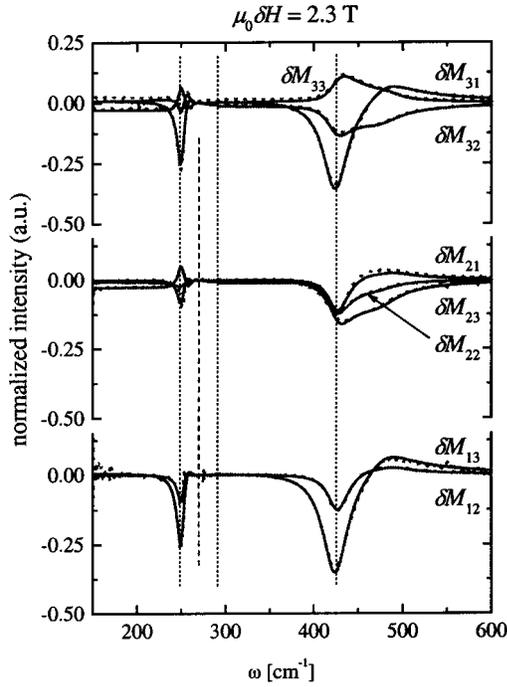
Fig. 3. Same as Fig. 2 but with the magnetic field perpendicular to the sample surface turned on and the spectra subtracted by the spectra shown in Fig. 2 (all spectra are differences between those at $\mu_0 H = 2.3$ T and $H = 0$). Note the scale change to the left.

ternal field ($\Psi_{ps} = \Psi_{sp} = 0$ because $\epsilon_{xy} = 0$). As can be seen now, the i-GaAs film causes excitation of p- and s-polarized n-GaAs-i-GaAs interface-bound modes. Two s-polarized surface guided branches (SGW$^{+,-}$) occur at wave numbers near the coupled LPP modes of the n-type GaAs substrate. These modes are extremely sensitive to the plasma frequency and plasma broadening parameters. Using the parameters given in Table 1 and the MDF for the n-type GaAs substrate and the i-type GaAs buffer layer, one can easily prove that the denominator of the s-polarized Fresnel reflection coefficient r_s for a film–substrate system[15] has a sharp minimum at the SGW$^{+,-}$ frequencies, which depend on Φ_a and d. As will be discussed elsewhere, this wave is associated with an interface-bound radiation pattern.[11] Both modes can be recognized in Figs. 2–6 (vertical dotted lines: mode SGW$^-$ occurs at $\omega \sim 249$ cm^{-1}, mode SGW$^+$ occurs at $\omega \sim 424$ cm^{-1}). A p-polarized Fano-type surface polariton [FSP: vertical dotted line between those for modes SGW$^{+,-}$ (Ref. 42)], also known as the Berreman effect,[44] exists near the GaAs LO phonon wave number ω_{LO} (vertical dashed line). Comments on the Berreman effect in semiconductor/dielectric layer structures have already been given by Röseler,[6] Zollner,[45] and Humliček,[46] and detailed analysis of the dispersion equation will be given in Ref. 11. Note that modes FSP and SGW are inherent in the Fresnel equation as a consequence of Maxwell's postulates. The magnetic-field-induced changes seen in Fig. 3 are strongest near the above-mentioned SGW mode frequencies. The middle set of curves in Fig. 5 displays strong $p-s$ polarization conversion near the frequencies of the SGW$^{+,-}$ modes. (The amount of Ψ_{ps} and Ψ_{sp} serves as a measure of strength of the ability of the sur-

face to convert incident p-polarized light into s-light polarized light, and vice versa.[24]) Similar features can be seen from the lower set of curves, which contains the difference between the Ψ_{pp} spectra with and without external field. Note that the magnetic field does not affect the FSP mode, and none of the difference spectra contains any feature at the FSP mode frequency. The middle and lower sets of curves in Fig. 6 show spectra for Δ_{ps} and Δ_{sp}, which correspond to the Ψ_{ps} and Ψ_{sp} spectra depicted in Fig. 5. Both Δ_{ps} and Δ_{sp} spectra transform into those for $\mu_0 H = -2.3$ T upon inversion along the 90° line (not shown). The appearance seen in Fig. 6 is that of negatively charged carriers with sgn(q) = -1 because $H > 0$ there. Hence the behavior of Δ_{ps} and Δ_{sp} provides sensitivity to the sign of the charge carrier, and we note the analogy with the behavior of Δ_{ps} and Δ_{sp} obtained from chiral liquid-crystal layers, which there revealed the handedness of the chiral structure.[47]

For GaAs with almost-spherical energy bands, the conduction-band effective-mass tensor can be taken as an isotropic scalar. The value of the electron effective mass at the bottom of the Γ_{1c} conduction band in GaAs is well established ($m/m_0 = 0.067$).[48] For large carrier concentration, the Fermi energy is located within the conduction band, which is known to have slight nonparabolicity effects for $\mathbf{k} \neq \mathbf{0}$.[48] For $N > 10^{17}$ cm^{-3}, the effect of the nonparabolicity of the band on the conduction-band effective

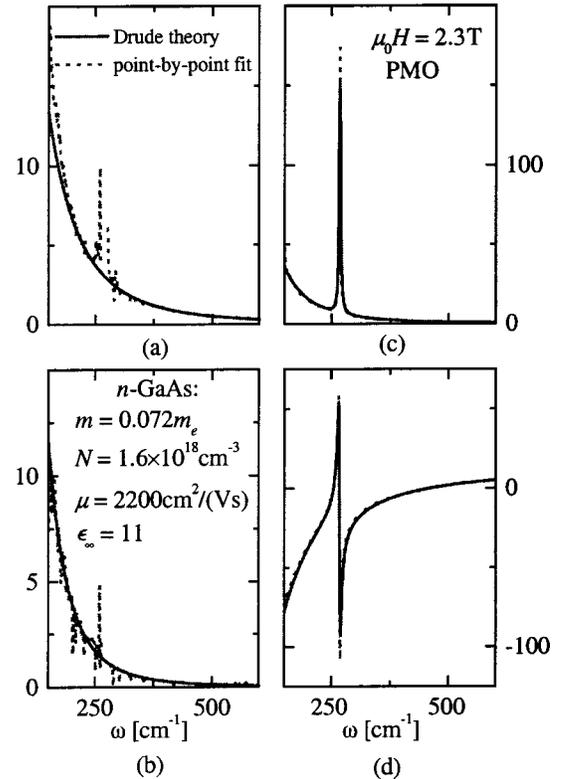Fig. 4. Wavelength-by-wavelength-inverted (dashed curves) and Drude-MDF best-fit (solid curves) far-infrared MO ϵ tensor element spectra ϵ_{xx} and ϵ_{xy} for the n-GaAs substrate obtained through model analysis of the experimental data shown in Fig. 5. The wavelength-by-wavelength-inverted spectra follow closely those predicted by Eqs. (15)–(17). (a) Im(ϵ_{xy}), (b) Re(ϵ_{xy}), (c) Im(ϵ_{xx}), (d) Re(ϵ_{xx}). The ϵ_{zz} spectra are virtually identical to the ϵ_{xx} spectra and are therefore omitted here.
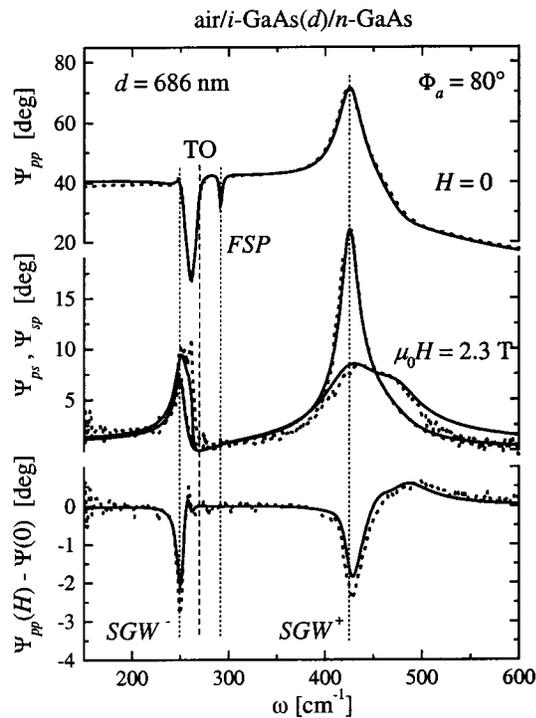
Fig. 5.   Experimental (dotted curves) and best-fit (solid curves) far-infrared MO generalized ellipsometry (normalized Jones matrix element) spectra for the i-GaAs(d)/n-GaAs homostructure at $\Phi_a = 80°$.   Upper set of curves: Ψ_{pp} at $H = 0$.   The dotted vertical lines indicate frequencies of the interface modes FSP, SGW$^+$, and SGW$^-$, discussed in the text.   The dashed vertical line denotes the wave number of the GaAs TO frequency. Middle set of curves: Ψ_{ps}, Ψ_{sp} at $\mu_0 H = 2.3$ T.   Lower set of curves: difference spectra $\Psi_{pp}(\mu_0 H = 2.3$ T$) - \Psi_{pp}(0)$.
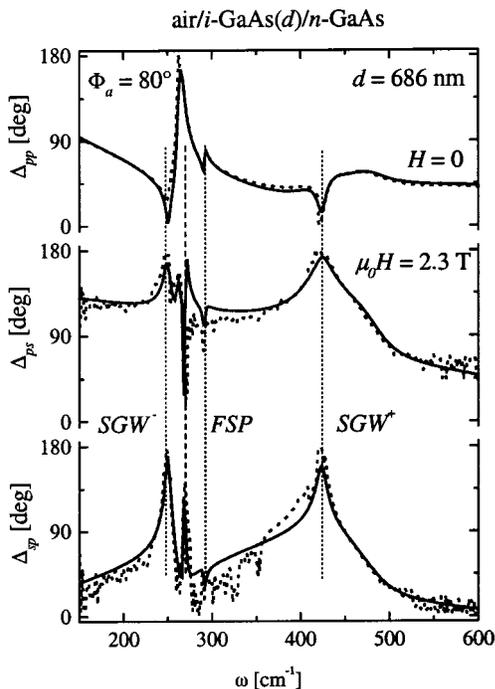
Fig. 6.   Same as Fig. 5 but for delta spectra.   Upper set of curves: Δ_{pp} at $H = 0$, middle set of curves: Δ_{ps} at $\mu_0 H = 2.3$ T, lower set of curves: Δ_{sp} at $\mu_0 H = 2.3$ T.

mass is not negligible, and m becomes a function of N. The best-fit free-carrier parameters obtained here for N and m are in excellent agreement with a solution of the three-level Kane equation derived by Raymond *et al.*[48] and also with data from low-temperature Shubnikov–de Haas and Faraday rotation experiments.   Data for n-type GaAs were compiled from the literature and given with their references in Ref. 48.   The set (N, m) obtained here agrees excellently with that expected for n-type GaAs. Therefore the far-infrared MO generalized ellipsometry technique has been demonstrated as an optical technique for measurement of the "inertial" mass of free-charge carriers in semiconductor materials.   We note, finally, that the generalized ellipsometry approach may likewise be used for precise measurement of the actual magnetic field strength by employing a material with well-known effective mass.

5.   SUMMARY

We demonstrated application of generalized ellipsometry at far-infrared wavelengths for measurement of the anisotropic MO response of semiconductor layered structures, exemplary for an i-GaAs/n-GaAs sample.   We determined wavelength by wavelength the MO dielectric function tensor elements of the n-type GaAs substrate upon numerical reduction of the undoped overlayer effect from the experimental data.   It was shown that the parameters m, μ, and N can be determined, independent of one another, from the spectral behavior of the wavelength-by-wavelength-extracted dielectric tensor element spectra upon matching the latter with the line shapes predicted by the Drude equation.   Hence a noncontact optical measurement can provide the desired information, avoiding the need to make electrical contacts otherwise necessary for Hall-effect measurements.   Samples with highly resistive overlayers, inaccessible to Hall-effect measurements, can also be studied.   The free-electron mass and mobility parameters for GaAs obtained here are in excellent agreement with results derived from previous Hall-effect and Shubnikov–de Haas experiments on bulk samples.   MO generalized ellipsometry may open up new avenues for nondestructive characterization of free-carrier properties in complex organic or inorganic semiconductor material heterostructures.

REFERENCES AND NOTES

1. The effective-mass concept addressed here descends from the similarity with the Newton force equation (acceleration of a body with mass m) and the acceleration experienced by a Bloch electron due to an external force. The inverse tensor obtained thereby depends on the curvature of the plots of electron energetic states versus electron momentum, which is diagonal by a suitable choice of axes. Different experiments require different concepts, resulting in definition of the effective conductivity mass, the density-of-states effective mass, the Hall effective mass, or the cyclotron effective mass, all of which are not discussed here. For the material investigated here (GaAs), the response of the zinc-blended, Γ-point conduction band (single-species, i.e., single-valley) Bloch electrons studied at infrared wavelengths is on a time scale much smaller than the average time between scattering events of the free electrons. One may also refer to the effective mass here as an (infrared) optical effective mass. See also Refs. 2 and 3.
2. C. M. Wolfe, N. Holonyak, Jr., and G. E. Stillmann, *Physical Properties of Semiconductors* (Prentice-Hall, Englewood Cliffs, N.J., 1989).
3. C. R. Pidgeon, "Free carrier optical properties of semiconductors," in *Handbook of Semiconductors*, M. Balkanski, ed. (North-Holland, Amsterdam, 1980), Vol. 2, pp. 223–228.
4. P. Drude, *The Theory of Optics*, translated from German by C. R. Mann and R. A. Millikan (Longmans, Green, New York, 1902).
5. H. Raether, *Surface Polaritons* (Springer, Berlin, 1988).
6. A. Röseler, *Infrared Spectroscopic Ellipsometry* (Akademie, Berlin, 1992).
7. J. J. Brion, R. F. Wallis, A. Hartstein, and E. Burstein, "Theory of magnetoplasmons in semiconductors," Phys. Rev. Lett. **28**, 1455–1458 (1972).
8. J. J. Brion, R. F. Wallis, A. Hartstein, and E. Burstein, "Interaction of surface magnetoplasmons and surface optical phonons in polar semiconductors," Surf. Sci. **34**, 73–80 (1973).
9. A. Hartstein, E. Burstein, J. J. Brion, and R. F. Wallis, "Surface polaritons on semi-infinite anisotropic media," Surf. Sci. **34**, 81–89 (1973).
10. R. F. Wallis, J. J. Brion, E. Burstein, and A. Hartstein, "Theory of surface polaritons in anisotropic dielectric media with application to surface magnetoplasmons in semiconductors," Phys. Rev. B **9**, 3424–3437 (1974).
11. M. Schubert, "Infrared ellipsometry on III-V semiconductor layer structures," Habilitationsschrift (Universität Leipzig, Leipzig, Germany), available at http://www.uni-leipzig.de/~hlp/ellipsometrie.
12. G. B. Wright and B. Lax, "Magnetoreflection experiments in intermetallics," J. Appl. Phys. **32**, 2113–2117 (1961).
13. M. Cardona, "Electron effective masses of InAs and GaAs as a function of temperature and doping," Phys. Rev. **121**, 752–758 (1961).
14. Restrictions apply to highly conductive layers that are optically thick, such as highly doped semiconductor substrates, or metal films several hundreds of nanometers thick. As long as the layer with high free-carrier concentration is passing electromagnetic radiation on to the next constituent, the ellipsometric parameters will contain information about the buried layers.
15. R. M. A. Azzam and N. M. Bashara, *Ellipsometry and Polarized Light* (North-Holland, Amsterdam, 1984).
16. D. E. Aspnes, "The accurate determination of optical properties by ellipsometry," in *Handbook of Optical Constants of Solids*, E. D. Palik, ed. (Academic, New York, 1998), Vol. I, pp. 89–112.
17. R. M. A. Azzam and N. M. Bashara, "Generalized ellipsometry for surfaces with directional preference: application to diffraction gratings," J. Opt. Soc. Am. **62**, 1521–1523 (1972).
18. M. Schubert, B. Rheinländer, B. Johs, C. M. Herzinger, and J. A. Woollam, "Extension of rotating analyzer ellipsometry to generalized ellipsometry: determination of the dielectric function tensor from uniaxial TiO_2," J. Opt. Soc. Am. A **13**, 875–883 (1996).
19. G. E. Jellison, Jr. and L. A. Boatner, "Optical functions of uniaxial ZnO determined by generalized ellipsometry," Phys. Rev. B **58**, 3586–3589 (1998).
20. D. W. Thompson, M. J. De Vries, T. E. Tiwald, and J. A. Woollam, "Determination of optical anisotropy in calcite from ultraviolet to mid-infrared by generalized ellipsometry," Thin Solid Films **313-314**, 341–346 (1998).
21. M. Schubert, T. E. Tiwald, and J. A. Woollam, "Explicit solutions for the optical properties of arbitrary magneto-optic materials in generalized ellipsometry," Appl. Opt. **38**, 177–187 (1999).
22. M. Schubert and C. M. Herzinger, "Ellipsometry on anisotropic materials: Bragg conditions and phonons in dielectric helical thin films," Phys. Status Solidi A **188**, 1563–1575 (2001).
23. M. Schubert and W. Dollase, "Generalized ellipsometry for biaxial absorbing minerals: determination of crystal orientation and optical constants from Sb_2S_3," Opt. Lett. **27**, 2073–2075 (2002).
24. M. Schubert, "Theory and application of generalized ellipsometry," in *Handbook of Ellipsometry*, G. E. Irene and H. W. Tompkins, eds. (to be published).
25. M. Schubert, B. Rheinländer, B. Johs, and J. A. Woollam, "Application of generalized ellipsometry to complex optical systems," in *Polarimetry and Ellipsometry*, M. Pluta and T. R. Wolinsky, eds., Proc. SPIE **3094**, 255–265 (1997).
26. M. Schubert, "Generalized ellipsometry and complex optical systems," Thin Solid Films **313-314**, 323–332 (1998).
27. M. Schubert, A. Kasic, T. Hofmann, V. Gottschalch, J. Off, F. Scholz, E. Schubert, H. Neumann, I. J. Hodgkinson, M. D. Arnold, W. A. Dollase, and C. M. Herzinger, "Generalized ellipsometry of complex mediums in layered systems," in *Complex Mediums III: Beyond Linear Isotropic Dielectrics*, A. Lakhtakia, G. Dewar, and M. W. McCall, eds., Proc. SPIE **4806**, 264–276 (2002).
28. This set comprises six real-valued quantities out of the eight possible values contained within the Jones matrix— lacking the light beam's absolute intensity and absolute phase information. For a definition of the Jones matrix elements, see Refs. 15, 17, 18, 24–27, and references therein.
29. G. E. Jellison, Jr., "Spectroscopic ellipsometry data analysis: measured versus calculated quantities," Thin Solid Films **313-314**, 33–39 (1998).
30. C. M. Herzinger, P. G. Snyder, B. Johs, and J. A. Woollam, "InP optical constants between 0.75 and 5.0 eV determined by variable-angle spectroscopic ellipsometry," J. Appl. Phys. **77**, 1715–1724 (1995).
31. M. Schubert, "Polarization-dependent optical parameters of arbitrarily anisotropic homogeneous layered systems," Phys. Rev. B **53**, 4265–4274 (1996).
32. T. E. Tiwald and M. Schubert, "Measurement of rutile TiO_2 from 0.148 to 33 μm using generalized ellipsometry," in *Optical Diagnostic Methods For Inorganic Materials II*, L. M. Hanssen, ed., Proc. SPIE **4103**, 19–29 (2000).
33. R. Henn, C. Bernhard, A. Wittlin, M. Cardona, and S. Uchida, "Far infrared ellipsometry using synchrotron radiation: the out-of-plane response of $La_{2-x}Sr_xCuO_4$," Thin Solid Films **313-314**, 643–648 (1998).

34. J. Kircher, R. Henn, M. Cardona, P. L. Richards, and G. P. Williams, "Far-infrared ellipsometry using synchrotron radiation," J. Opt. Soc. Am. B **14**, 705–712 (1997).

35. J. Humlíček, R. Henn, and M. Cardona, "Infrared vibrations in LaSrGaO$_4$ and LaSrAlO$_4$," Phys. Rev. B **61**, 14554–14563 (2000).

36. T. E. Tiwald, J. A. Woollam, St. Zollner, J. Christiansen, R. B. Gregory, T. Wetteroth, and S. R. Wilson, "Carrier concentration and lattice absorption in bulk and epitaxial silicon carbide determined using infrared ellipsometry," Phys. Rev. B **60**, 11464–11474 (1999).

37. M. Schubert, T. E. Tiwald, and C. M. Herzinger, "Infrared dielectric anisotropy and phonon modes of sapphire," Phys. Rev. B **61**, 8187–8201 (2000).

38. A. Kasic, M. Schubert, S. Einfeldt, D. Hommel, and T. E. Tiwald, "Free-carrier and phonon properties of n- and p-type hexagonal GaN films measured by infrared ellipsometry," Phys. Rev. B **62**, 7365–7377 (2000).

39. C. Kittel, *Introduction to Solid State Physics* (Wiley, New York, 1985).

40. In view of the generalized ellipsometry applications at oblique incidence, MO setups will be addressed as follows: the polar MO (PMO) setup with **B** parallel to the sample normal, the longitudinal MO (LMO) setup with **B** parallel to the sample surface and parallel to the plane of incidence, and the transverse MO (TMO) setup with **B** perpendicular to the sample normal and perpendicular to the plane of incidence. In the MO literature, different terms are in use: Near-normal-incidence reflection-type Kerr-effect measurements are referred to as transverse, longitudinal, and polar configurations, in conceptual agreement with the above notation. Faraday- and Voigt-effect measurements address transmission-type linear polarization rotation measure-ments in the above PMO and mixed LMO–TMO configurations, respectively. See Ref. 3 or Ref. 41. These configurations mostly result from the simplicity of the corresponding equations, which describe the polarized light reflection and transmission situations for the anisotropic materials. These requirements are now dispensed with because of the availability of explicit solutions for light propagation in arbitrarily nonsymmetric (MO) dielectric materials.[21]

41. M. Mansuripur, *The Physical Principles of Magneto-Optical Recording* (Cambridge U. Press, Cambridge, UK, 1995).

42. E. D. Palik, "Gallium arsenide (GaAs)," in *Handbook of Optical Constants of Solids*, E. D. Palik, ed. (Academic, New York, 1998), Vol. I; pp. 429–444.

43. E. Burstein and F. De Martini, eds., *Polaritons* (Pergamon, New York, 1974).

44. D. W. Berreman, "Infrared absorption at longitudinal optic frequency in cubic crystal films," Phys. Rev. **130**, 2193–2198 (1963).

45. St. Zollner, J. P. Carrejo, T. E. Tiwald, and J. A. Woollam, "The origin of the Berreman effect in SiC homostructures," Phys. Status Solidi B **208**, R3–R4 (1998).

46. J. Humlíček, "Infrared spectroscopy of LiF on Ag and Si," Phys. Status Solidi B **215**, 155–159 (1999).

47. M. Schubert, B. Rheinländer, C. Cramer, H. Schmiedel, J. A. Woollam, B. Johs, and C. M. Herzinger, "Generalized transmission ellipsometry for twisted biaxial dielectric media: application to chiral liquid crystals," J. Opt. Soc. Am. A **13**, 1930–1940 (1996).

48. A. Raymond, J. L. Robert, and C. Bernard, "The electron effective mass in heavily doped GaAs," J. Phys. C **12**, 2289–2293 (1979).